Original

Schober, M.; Eidenberger, E.; Staron, P.; Leitner, H.:

Critical Consideration of Precipitate Analysis of Fe–1 at.% Cu Using Atom Probe and Small-Angle Neutron Scattering

In: Microscopy and Microanalysis (2010) Cambridge University Press

DOI: 10.1017/S1431927610093955

Microsc. Microanal. 17, 26–33, 2011
doi:10.1017/S1431927610093955

Microscopy AND Microanalysis

Critical Consideration of Precipitate Analysis of Fe–1 at.% Cu Using Atom Probe and Small-Angle Neutron Scattering

M. Schober,[1,*] E. Eidenberger,[1] P. Staron,[2] and H. Leitner[1]

[1]*Department of Physical Metallurgy and Materials Testing, University of Leoben, Franz-Josef-Straße 18, 8700 Leoben, Austria*
[2]*Institute of Materials Research, GKSS Research Centre, Max Planck-Str. 1, 21502 Geesthacht, Germany*

Abstract: An Fe–1 at.% Cu model alloy was examined by atom probe (3DAP) and small-angle neutron scattering (SANS) to verify the accordance of the gained results. The Fe-Cu alloy was heat-treated for various times at 500°C, forming Cu-rich precipitates within the Fe matrix. The chemical compositions of the precipitates and matrix found by 3DAP were used to calculate the magnetic scattering contrast. Additionally, a magnetic moment of the precipitates that contain a significant amount of Fe was taken into account for the calculation of magnetic scattering contrast. This in turn is used for the evaluation of the magnetic scattering curves gained by SANS. Both the 3DAP data as well as the scattering curves were analyzed with regard to radius, number density, and volume fraction of the precipitates as a function of aging time. The results yielded by both techniques are in good agreement and correspond to the development of the hardness of the alloy. Minor differences can be related to the cluster search algorithm used for the analysis of the 3DAP data as well as Fe overestimation based on different field phases.

Key words: atom probe, small-angle neutron scattering, precipitation reaction, Fe-Cu alloy

Introduction

The precipitation reaction of Cu in pure Fe and steels was extensively studied in the past, especially because of the use of such alloys in pressure vessel steels (Pareige et al., 1995, 1996, 1997*a*, 1997*b*; Pareige & Miller, 1996). The precipitation reaction in the Fe-Cu system was first reported by Smith and Palmer (1933). Early work was carried out to study the precipitation reaction in an Fe 1.23 wt% Cu alloy by Hornbogen and Glenn (1960). Hornbogen found out that the Cu clusters initially precipitate with a metastable [body-centered cubic (bcc)] structure coherent with the matrix capturing a spherical shape. A change into rod-shaped particles with a stable incoherent [face-centered cubic (fcc)] structure occurs at a radius of approximately 5 nm (Hornbogen, 1962). Similar experimentally determined threshold values for the structure change (5–9 nm) were reported by several other authors (Lahiri et al., 1969; Goodman et al., 1973*a*; Dahmen et al., 1984). Theoretical calculations revealed a critical size of approximately 4 nm (Goodman et al., 1973*b*). In 1991 Othen et al. stated that the transformation of (bcc) Cu precipitates into the (fcc) structure proceeds over a martensitic transformation with a 9R structure.

The composition development of the Cu precipitates was also extensively studied over the years, but no clear conclusions were drawn. Hornbogen (1962) suggested that the evolving (bcc) Cu cluster consists of 100 at.% Cu; however, at that time there was no experimental proof. The first atom probe measurements by Goodman et al. (1973*b*) showed that precipitated particles only contain 50 at.% Cu at the early stages. These findings were supported by various atom probe measurements carried out in the last 20 years (Pareige et al., 1996; Pareige & Miller, 1996; Miller et al., 2000; Isheim & Seidman, 2004; Isheim et al., 2006; Prakash Kolli & Seidman, 2008). In contrast, the evaluations of small-angle neutron scattering (SANS) data were usually based on the assumption of completely nonmagnetic (bcc) Cu precipitates resulting in a Cu content of nearly 100 at.% (Worrall et al., 1987; Osamura et al., 1993). Even though density functional theory (DFT) calculations showed that Cu precipitates exhibit a magnetic moment if Fe is incorporated (Zhang & Ma, 2000; Liu et al., 2005), it was not considered in SANS data evaluations.

The sequence of precipitation, structure, and composition was studied by comparing various techniques such as, e.g., atom probe (Goodman et al., 1973*a*; Worrall et al., 1987; Pareige et al., 1996), transmission electron microscopy (Charleux et al., 1996; Maruyama et al., 1999), and small-angle X-ray scattering (Deschamps et al., 2001). Miller et al. (2003) compared three-dimensional atom probe (3DAP) and SANS measurements on neutron irradiated Fe-Cu alloys. They were able to find good agreement for the precipitate characteristics radius and number density, but unsolved discrepancies occurred concerning the volume fraction and chemical composition of the clusters. They assumed that the Cu precipitates with incorporated Fe do not carry a magnetic moment. Consequently, the measured and calculated ratio of magnetic to nuclear scattering contrast between clusters and matrix do not match at all. Therefore, a closer look on these deviations is necessary to find reasonable approaches in data evaluation for both techniques.

Received February 4, 2010; accepted August 10, 2010
*Corresponding author. E-mail: michael.schober@mu-leoben.at

Table 1. Composition of the Investigated Model Alloy Measured by Emission Spectral Analysis (ESA).

	Cu	C	Cr	Si	Mn	Ni	O	N	Fe
at.%	0.986	0.008	0.014	0.02	0.034	0.015	0.335	0.075	98.513

Recently, the authors of this study (Schober et al., 2010) showed that the SANS data evaluation, including magnetic moments calculated by DFT, fits excellently with the gained results from atom probe, suggesting that Cu precipitates consist of approximately 50 at.% Cu in the early aging states.

In this article 3DAP and SANS results obtained from the early aging states of an Fe–1 at.% Cu alloy are presented and analyzed. The aim is to compare these two complementary methods in terms of radius r, number density N, and volume fraction f, when the SANS data evaluation considers a magnetic moment of the occurring precipitates (Schober et al., 2010) based on the chemical composition found by 3DAP. The conducted atom probe measurements are generally improved compared to former works in case of analyzed volume size and therefore detected number of precipitates. The method of comparing both techniques via the chemical composition found by 3DAP is described, and problems during data analysis and their reproducibility are discussed.

Materials and Methods

A 10 kg Fe–1 at.% Cu alloy was vacuum induction melted and cast under vacuum. The chemical composition as measured with emission spectral analysis (ESA) is given in Table 1. The ingot was cut into $15 \times 15 \times 50$ mm^3 bars for the subsequent heat treatment. The bars were solution annealed at 850°C for 60 h, water quenched, and aged at 500°C for several times. The hardness was measured using Vickers hardness indentations with 10 kg load as a function of aging time at 500°C (Fig. 1). From this hardness curve designated aging times for the 3DAP and SANS experiments—namely, 5,000, 10,000, 30,000, and 100,000 s—were selected.

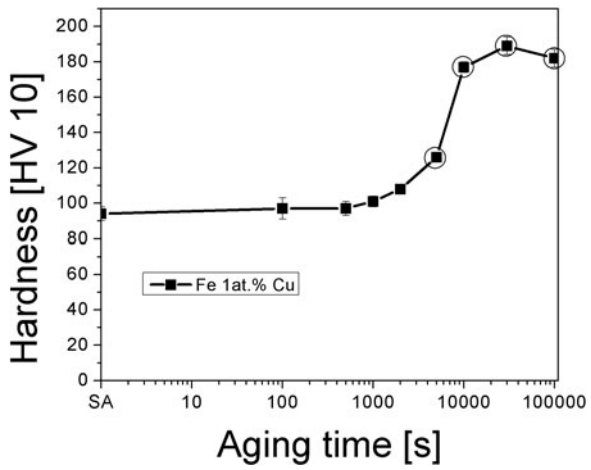

Figure 1. Hardness (HV10) over aging time curve generated for the Fe–1 at.% Cu alloy. The circles denote the selected aging states for further analysis.

Three-Dimensional Atom Probe

The atom probe investigations were performed on an energy compensated 3D atom probe 3DAP^{TM}–X provided by Oxford Nanoscience (Milton Keynes, UK). The analysis conditions of 60 K, a pulse fraction of 20%, and a pulse repetition rate of 20 kHz were used. The needle-shaped specimens were assembled by the standard two-step etching technique (Miller, 1996). For step one 15% perchloric and 85% acetic acid and for step two 2% perchloric acid in butoxyethanol were used. The data reconstruction was performed on the visualization program IVAS 3.4.1 provided by Imago^{TM} (now CAMECA, Madison, WI, USA). The particle identification was done by a cluster search algorithm based on the maximum separation method (Vaumousse et al., 2003; Cerezo & Davin, 2007). The parameter d_{max} is the maximum separation distance between the solute atoms. The parameter N_{min} gives the minimum number of solute atoms defining a cluster. This number should not be too small to ensure that no random fluctuations count as clusters. On the contrary, too high values for N_{min} reduce the efficiency of the cluster search algorithm (Vaumousse et al., 2003). For this alloy the parameter d_{max} was set to 0.6 nm and N_{min} to 10 assign using the procedure reported by Vaumousse et al. (2003). Finally, the supplemental parameter envelope distance L and the erosion distance d_{ero} are set to the same values as d_{max}. The distance distribution between the cluster centers was calculated for each cluster, found by the cluster search algorithm, using the smallest average center-to-center distance.

Small-Angle Neutron Scattering

The SANS experiments were carried out at the instrument SANS-2 at the Geesthacht Neutron Facility (GeNF) at GKSS in Geesthacht, Germany. The measurements were performed on disc-shaped samples of 2 mm thickness and 18 mm diameter at room temperature under a saturating magnetic field of 2 T. Unpolarized neutrons with a wavelength of $\lambda = 0.58$ nm and a wavelength spread of $\Delta\lambda/\lambda = 10\%$ were used. The exposure time of the samples in the neutron beam with an impinging diameter of 8 mm was set to 15 min for all measured samples. The nuclear and magnetic scattering curves were extracted separately from the two-dimensional detector image using sectors with an opening angle of 10° parallel and perpendicular to the applied magnetic field. The scattering curves were corrected for sample transmission and background noise. The quantification of scattering cross sections was performed by a vanadium standard calibration. The magnetic scattering curve gained from the solution-annealed sample was subtracted

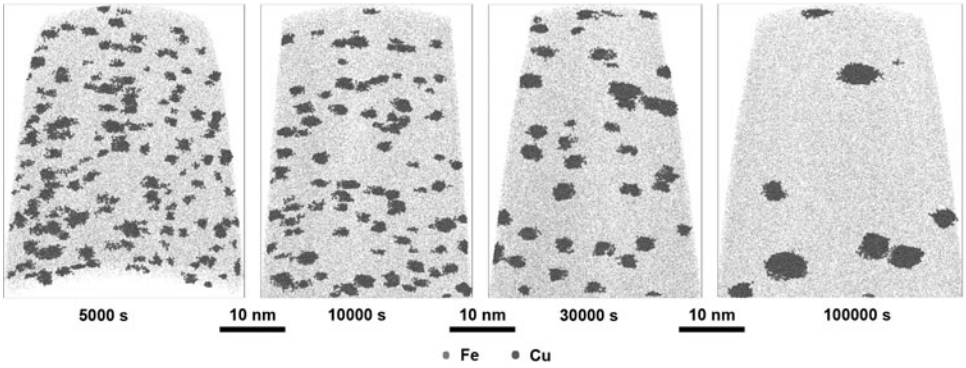

Figure 2. Three-dimensional reconstructions gained by 3DAP of the different aged samples at 500°C: (**a**) 5,000 s, (**b**) 10,000 s, (**c**) 30,000 s, and (**d**) 100,000 s.

from all aged samples to reduce the influence of possible larger scattering structures (Mathon et al., 1997). The resulting scattering curves were fitted by means of a two-phase model concerning radius r, number density N, and volume fraction f of the precipitates (Kostorz, 1979):

$$\left(\frac{d\Sigma}{d\Omega}\right)_{mag}(q) = (\Delta\eta)^2_{mag}\int_0^\infty n(R)V(R)^2F(q,R)^2\,dR. \quad (1)$$

In equation (1) $d\Sigma/d\Omega$ represents the macroscopic magnetic scattering cross section, $\Delta\eta_{mag}$ is the magnetic scattering contrast, $n(R)dR$ stands for the number density of particles between R and $R + dR$, $V(R)$ is the volume of the particles, and $F(q,R)$ is the form factor F of spherical particles:

$$F(q,R) = 3\left(\frac{(\sin qR - qR\cos qR)}{(qR)^3}\right). \quad (2)$$

The matrix and the developed particles have different chemical compositions and hence different magnetic scattering length densities ($\eta_{mag,m}$, $\eta_{mag,p}$). This leads to the magnetic scattering length density difference $\Delta\eta_{mag}$, which can be theoretically calculated via equation (3):

$$\Delta\eta_{mag} = \eta_{mag,m} - \eta_{mag,p} = p_0\left[\left(\frac{\mu_m}{V_m}\right) - \left(\frac{\mu_p}{V_p}\right)\right]. \quad (3)$$

The gyromagnetic ratio $p_0 = 2.7\cdot10^{-13}$ cm/μB (Bacon, 1975) is used for the calculation as well as the magnetic moments of matrix μ_m and particles μ_p, which are derived from the chemical composition gained by 3DAP combined with DFT calculations (Schober et al., 2010). The atomic volumes (V_m, V_p) are calculated using lattice constants found by DFT calculations as well. The results obtained from these $\Delta\eta_{mag}$ calculations were applied in equation (1) to fit the magnetic scattering curves in an appropriate way.

Results

A hardness over aging time curve was mapped to define the aging states for further 3DAP and SANS investigations. Figure 1 shows the hardness as a function of aging time at 500°C. After approximately 1,000 s the first slight hardness increase is measurable. The hardness increases to a maximum after 30,000 s of aging and shows a decrease at 100,000 s. The selected aging states for analyzing are 5,000, 10,000, 30,000, and 100,000 s.

The 3D reconstructions of the atom probe measurements for the selected aging states are shown in Figure 2. For a better visualization only 5% of all measured Fe atoms are shown, while all Cu atoms are included with an increased size. The depicted 3D volumes are clipped to similar sizes ($40 \times 40 \times 50$ nm^3) for better comparability. The effectively analyzed volumes are listed in Table 2. By an optical inspection, Cu clusters and their size development over aging time can be observed. Additionally, an increase of the distance between the clusters centers found by the cluster search algorithm with aging time can be seen that is confirmed by the values of the cluster search results in Table 2. The 3D particle center distance increases with a factor of 3 from 5.2 to 15.6 nm, and the radius increases as

Table 2. Radius, Particle Distance, Analyzed Volume, Composition of the Found Precipitates Measured with 3DAP.

Aging Time (s)	Particle Radius (nm)	Particle Distance (nm)	Analyzed Volume (nm^3)	Composition of Matrix Cu (at.%)	Composition of Precipitates Cu (at.%)	Composition of Precipitates Fe (at.%)
5,000	1.08 ± 0.28	5.2 ± 1.7	93,500	0.7 ± 0.05	46.9 ± 0.45	53.1 ± 0.40
10,000	1.23 ± 0.41	6.5 ± 2.2	454,235	0.45 ± 0.03	47.6 ± 0.18	52.4 ± 0.16
30,000	2.02 ± 0.55	9.1 ± 2.9	303,499	0.3 ± 0.03	48.4 ± 0.18	51.6 ± 0.17
100,000	3.2 ± 1.1	15.6 ± 5.7	639,394	0.19 ± 0.02	51.7 ± 0.16	48.3 ± 0.18

Table 3. Magnetic Moments of Matrix and Precipitates Gained by DFT Calculations are Shown.*

Aging Time (s)	μ_m (μB)	μ_p (μB)	$\Delta\eta_{mag}$ (10^{10} cm^2)
5,000	2.176	1.31	2.62
10,000	2.181	1.3	2.72
30,000	2.185	1.28	2.90
100,000	2.187	1.2	3.22

*The magnetic scattering contrasts for the SANS curve evaluations are presented.

well with a factor of 3 from 1.08 to 3.2 nm over aging time. The chemical composition of the clusters is also shown in Table 2. A slight increase over aging time from 46.9 at.% Cu up to 51.7 at.% Cu in the precipitates, found by the cluster search algorithm, can be observed. These compositions and the magnetic moments obtained by DFT (Schober et al., 2010) (Table 3) are used for the calculations of $\Delta\eta_{mag}$ [equation (2)], which are further used for the SANS curve evaluation [equation (1)]. The magnetic scattering contrast $\Delta\eta_{mag}$ exhibits, as it is calculated with the magnetic moment of the precipitates, an enhancement over the aging time from $2.66 \cdot 10^{10}$ up to $3.2 \cdot 10^{10}$ cm^2 (Table 3).

Figure 3 presents a series of magnetic scattering curves measured on the Fe–1 at.% Cu alloy. The bottom curve shows the solution-annealed sample that was used as a reference. With increasing aging time the scattering cross section increases. The scattering intensity shifts toward smaller q-values with increasing aging time. The dashed lines are the results of the two-phase curve fits [equation (1)] of each individual scattering curve.

Figure 4 provides the development of average particle radius r, number density N, and volume fraction f over aging time determined by 3DAP (full squares) and SANS (full circles). The results gained by SANS were evaluated using equation (1) and the calculated $\Delta\eta_{mag}$ listed in Table 3. Starting at 5,000 s the found radius for both techniques

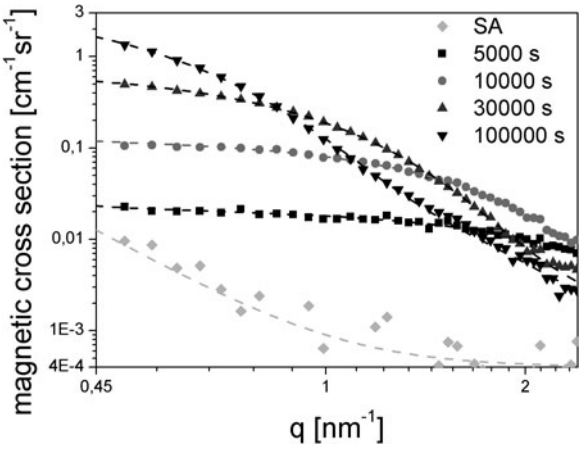

Figure 3. Development of the magnetic scattering curves with aging time at 500°C. The calculated curves are shown as dashed lines.

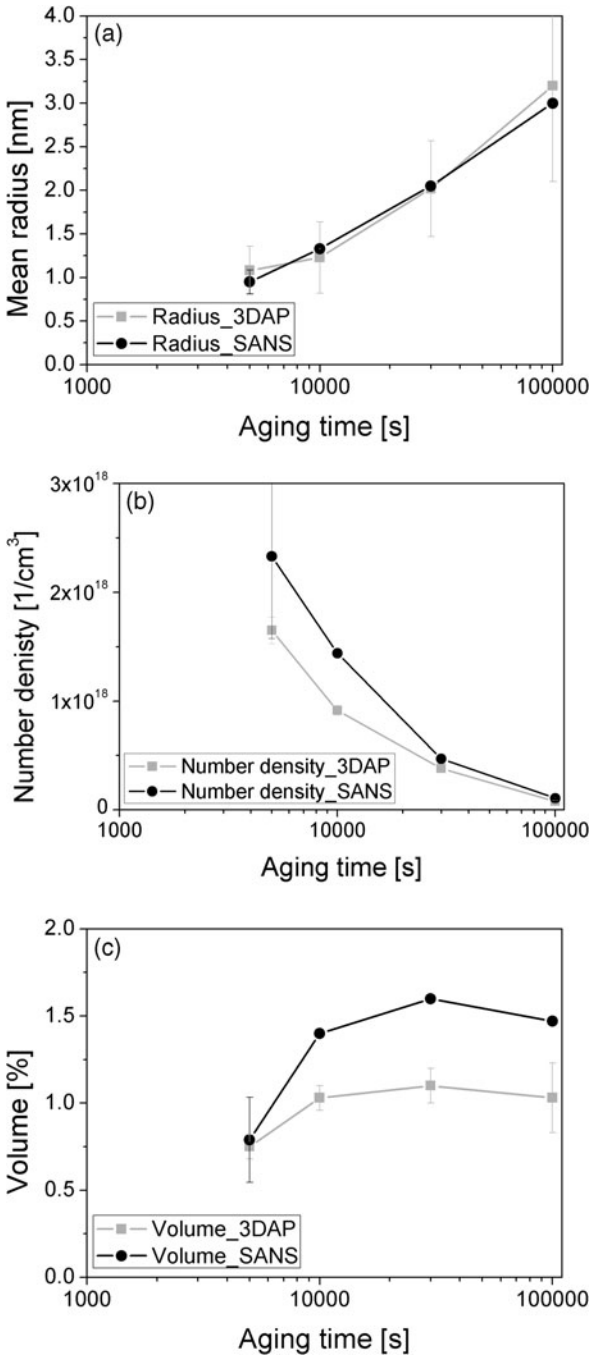

Figure 4. Development of (**a**) radius, (**b**) number density, and (**c**) volume fraction over aging time as obtained by 3DAP and SANS. The SANS data were evaluated using the magnetic scattering length density difference calculated from the chemical composition found by 3DAP (Table 3).

captures a value of about 1 nm and increases up to approximately 3 nm. It should be noted that the error bars for the mean radii gained by 3DAP gradually increase while the error bars of the SANS results, due to the data quality and fit results of the SANS curve, are within the symbol size. The error, which is caused by calculation of the magnetic scattering length density difference $\Delta\eta_{mag}$ and further the chemical composition found by 3DAP, is not indicated. The

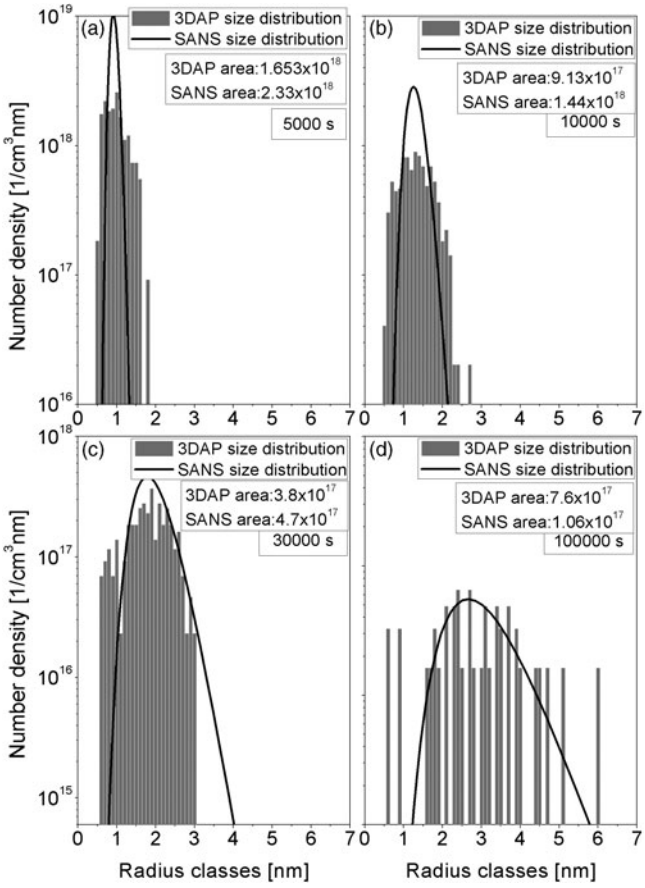

Figure 5. Size distributions in terms of number density for the selected aging times: (**a**) 5,000 s, (**b**) 10,000 s, (**c**) 30,000 s, and (**d**) 100,000 s.

number densities (Fig. 4b) for both analysis techniques show the same trend starting at high values of about $1.65 \cdot 10^{18}$ (1/cm^3) and $2.33 \cdot 10^{18}$ (1/cm^3) for 3DAP and SANS, respectively. The values drop down over aging time and capture nearly the same values after 100,000 s aging—namely, $7.6 \cdot 10^{16}$ (1/cm^3) for 3DAP and $1.06 \cdot 10^{17}$ (1/cm^3) for SANS. The volume fraction (Fig. 4c) also shows the same characteristics for both techniques; however, the volume fractions found by SANS are a factor 1.5 higher compared to the results gained by 3DAP. Only the shortest aged state (5,000 s) exhibits a satisfactory accordance for both applied analysis techniques.

Figure 5 displays the size distributions found by 3DAP and SANS for the selected aging times. The bar charts represent the 3DAP results, and the SANS results are illustrated by line charts. Additionally, the total number densities are given in Figure 5 as the integral of the distributions. The distributions of the 5,000 s and 10,000 s aged states in Figure 5a,b fit well in regard to the mean radius as well as the width of the distribution. However, the maximum values of the number densities are smaller as it is obvious in Figure 4b. The distributions of the 30,000 s and 100,000 s aged states match remarkably well in case of width and absolute values of the number density. Generally, the distributions obtained from both techniques are very similar.

Discussion

Nearly all existing studies on the system Fe-Cu using atom probe analysis report that the developing Cu clusters contain starting at approximately 50 at.% Fe with variations up to 70 at.% depending on aging temperature and time (Pareige et al., 1995; Miller et al., 2000; Isheim et al., 2006). Isheim et al. measured Cu precipitates, aged for 100 h at 500°C, which consist of 64 at.% Cu inside the precipitates using proximity histogram (Hellman et al., 2000). Miller et al. (2003) found Cu concentrations up to 65 at.% in the core of the precipitates after neutron irradiation. It has to be pointed out that the concentration calculated using cluster search algorithms, as done in this work, is an average over the core of the particle and the interface region. The found composition of the particles is methodically higher of matrix elements compared to results found inside the particles using proximity histograms. In the interface region between matrix and core of the precipitates, the Cu concentration increases rapidly over an infinitesimal small distance up to core composition. However, it is difficult to describe the exact size of this interface region because of different evaporation fields of matrix and precipitates. This leads to ion trajectory overlaps during the atom probe run and thus the measured atomic density, and chemical composition is influenced in the interface region. SANS, on the other hand, also yields results that are integrated over the whole particles with including the interface region. Gradients in chemical composition as well as magnetic moment from particle core to the edge of the particles lead to average form factors and the corresponding scattering curves. Hence, for comparing atom probe results with SANS results, it is necessary to use the chemical composition obtained by a cluster search algorithm. However, SANS data evaluation on the system Fe-Cu was always performed under the consideration of pure Cu precipitates, and consequently, they were treated as nonmagnetic (Osamura et al., 1993; Miller et al., 2003). The authors of the present work (Schober et al., 2010) showed that, if a significant magnetic moment of precipitates is taken into account, there is a correspondence between the results found by 3DAP and SANS in terms of calculated scattering contrasts and hence chemical composition.

Consequently, the magnetism of the Cu clusters has to be taken into account when the system Fe–1 at.% Cu is analyzed with regard to radius r, number density N, and volume fraction f. The 3D reconstructions and the cluster search algorithm results (Figs. 2, 4) revealed the precipitation development with aging time. It was shown that the average radius of the particles increases whereas the number density decreases, leading to a raised mean particle distance.

The number density obtained from 3DAP, especially at the earliest aging state, is about 30% smaller than the SANS result. This discrepancy can be explained by a critical consideration of the cluster search parameters. The parameter

N_{min} has to be chosen within a range that excludes random fluctuations on the one hand and guarantees a detection of very small clusters on the other hand. The detector efficiency of the used atom probe is approximately 35%, which leads to a minimally detectable particle size of 0.55 nm if N_{min} is set to 10 and under the simplified assumption of approximately 50 at.% Fe incorporated in the particles. Additionally, the measured SANS data, especially for the two early aging stages, are of limited quality because the covered q-range is relatively small. Therefore, the smallest cluster sizes cannot fully be resolved, which could also partly explain the deviations in the number density. With increasing aging time and hence increasing particle size, the accuracy of the number density found by 3DAP is increasing, which is obvious by observing Figure 4b. The number density found by 3DAP approaches the number density gained by SANS with increasing aging time. For all aging conditions measured with 3DAP, the precipitates, which are cut by the reconstructed volume, are counted adequately. The resulting influence on the number density should be small compared to the other mentioned influences.

By a closer inspection of the 3D reconstructions (Fig. 2), it seems that the clusters are not randomly distributed, especially for the 30,000 and 100,000 s aged samples, leading to inaccuracies in precisely defining the number density by the 3DAP data. To further check this, the frequency distribution of the clusters within the analyzed volume was calculated (Fig. 6) (Cerezo & Davin, 2007). Therefore, the analyzed volume is divided in a set of subvolumes of $20 \times 20 \times 20$ nm^3 and the frequency distribution of the clusters was calculated. For this, the coordinates of the centers of the clusters were used to determine their number within the analyzed volume. These distributions were compared to the Poisson distribution. The x-axis represents the count of clusters within a subvolume (block) and the y-axis the number of occurring blocks with the certain count of clusters. The squares represent the experimentally observed cluster frequency distribution and the lines show, based on the mean number observed, the calculated Poisson distributions. The early aging states 5,000 s and 10,000 s show χ^2 values that are 15 and 29, respectively. The prolonged aging states 30,000 s and 100,000 s exhibit calculated χ^2 values of 3 and 2.5, which give a significance of more than 99% with a degree of freedom of 19. The statistics of these distributions are poor, but dictated by the limits of current 3DAP techniques. Nevertheless, it can be seen that especially at the longest aged condition the cluster distributions satisfactorily obey a Poisson distribution. Such distribution describes an overall random occurrence, which is the case for precipitation reaction with low volume fractions (Cerezo & Davin, 2007). Thus, a completely inhomogeneous distribution can be excluded. The fact that there is still a relatively large discrepancy in the number density results of the complementary methods for the 5,000 s aged sample indicates the need for further investigations. The size distributions obtained from both methods for the 5,000 s aged sample look quite different (Fig. 5a). On the other hand, the size distributions

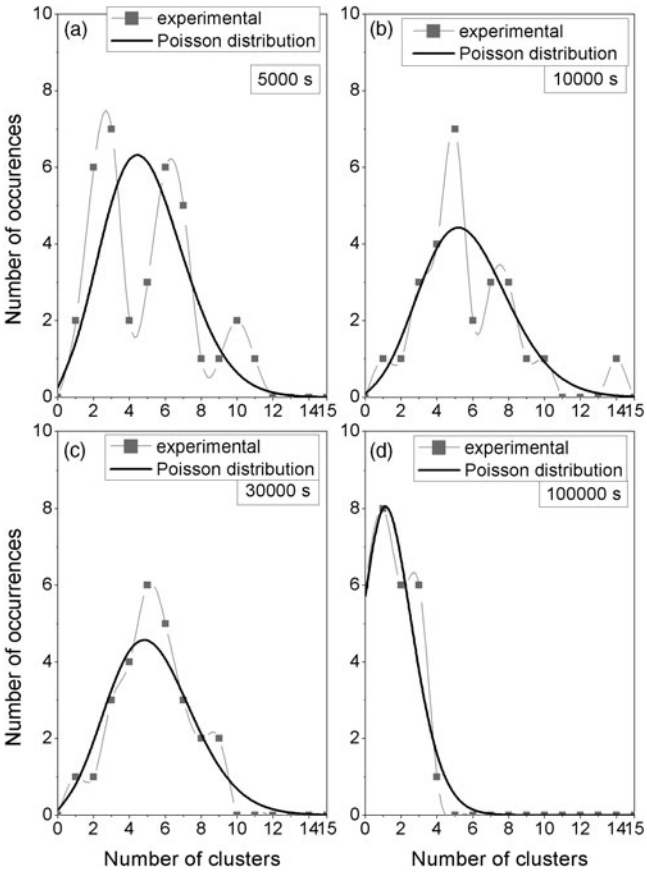

Figure 6. Cluster frequency distributions within box sizes of $20 \times 20 \times 20$ nm^3 calculated from the 3D reconstructions gained by 3DAP after different times of aging at 500°C: (**a**) 5,000 s, (**b**) 10,000 s, (**c**) 30,000 s, and (**d**) 100,000 s.

for the long aging states match quite well. This shows that both techniques detect almost the same number density of particles. The theoretical maximum precipitated volume fraction for the Fe–1 at.% Cu alloy is approximately 2%, considering the chemical composition of the precipitates found by 3DAP of approximately 50 at.% and with the simplification that Cu atoms capture the same volume in the alloy as Fe atoms. The maximum precipitated volume fraction of 1.6% gained by the SANS measurement of the 30,000 s aged state is close to the theoretical maximum volume fraction. However, this volume is a factor 1.5 higher compared to the result found by 3DAP. Under the consideration that the Fe content in the Cu precipitates decreases over the aging time, as shown in literature (Goodman et al., 1973*b*; Prakash Kolli & Seidman, 2008), the volume fraction found by SANS is significantly too high. The reason is based on the assumption that the precipitates reach almost 100 at.% Cu after prolong aging, and hence the maximum precipitated volume fraction reaches about 1%. However, the characteristics of both volume fraction curves are similar and also are consistent with the hardness curve (Fig. 1) in an appropriate way. The volume fraction increases up to the hardness maximum at 30,000 s indicating the end of the growth process (Haasen, 1978), and with the hardness de-

crease the volume fraction stays more or less constant. A possible explanation for the generally too high volume fraction of SANS can be found by the frequently reported overestimation of the Fe content in the precipitates by 3DAP and further too low magnetic scattering contrasts $\Delta\eta_{mag}$ (Leitner et al., 2004, 2007). Morley et al. (2009) showed that trajectory overlaps of the evaporated atoms at the interface of the Cu precipitates (low field phase) and the Fe matrix (high field phase) during the atom probe measurements can influence the analyzed atomic density and furthermore the chemical composition of the detected precipitates. Due to this fact, the Fe content in the precipitates may be overestimated, which would lead to higher magnetic scattering contrasts effecting the SANS evaluation. For the 30,000 s aged state, a reduction of the Fe content of 5 at.% in the precipitate would lead to a change in $\Delta\eta_{mag}$ from $2.9 \cdot 10^{10}$ to $3.2 \cdot 10^{10}$ resulting in a volume fraction of 1.38 vol% instead of 1.6 vol%. Such a change would lead to a smaller deviation of the volume fraction found by SANS and 3DAP. Additionally, by trend the volume fraction would sink under the theoretical calculated threshold of approximately 1% precipitated volume. Therefore, it seems very likely that overestimation of Fe plays an important role in this alloy.

In general, the results obtained from 3DAP and SANS in Fe–1 at.% Cu agree very well. On the one hand, 3DAP delivers compositional data that are required for quantitative SANS data analysis regarding precipitate number density and volume fraction (while it is not needed for determining precipitate sizes). On the other hand, SANS data yield good statistics due to the large volume inspected. The combination of both probes opens up new possibilities for both further development of the methods and the investigation of materials.

Conclusions

The well-known precipitation reaction of an Fe–1 at.% Cu model alloy was analyzed under magnetic consideration using atom probe (3DAP) and SANS to verify and assess the comparability of the results of these two techniques. The following conclusions can be drawn:

- The measured mean radius of the developing Cu precipitates shows a constant increase over aging time, and both analysis techniques have the ability to depict this behavior with an excellent accordance.
- The number density obtained by both 3DAP and SANS decreases over the analyzed aging time. The discrepancies between 3DAP and SANS results, especially at the early aging states, can be caused by the limited SANS data quality because of the relatively small covered q-range, leading to a reduced resolution of the smallest cluster sizes.
- The precipitated volume fractions qualitatively obtained from both techniques is consistent with the macroscopic hardness behavior in an appropriate way. However, like the number densities, the absolute values of both techniques still differ. Reasonable volume fractions, found by SANS, approaching the theoretically expected maximum were definitely only obtained by taking into account a magnetic moment of the precipitates calculated within the DFT and the chemical composition gained by 3DAP.

The combination of 3DAP and SANS opens up new possibilities for the study of precipitation kinetics because both deliver truly complementary results.

Acknowledgments

This work was supported by the Austrian science fund FWF under Grant No. P18480-N19. This research project has been supported by the European Commission under the 7th Framework Programme through the Research Infrastructures action of the Capacities Programme, Contract No: CP-CSA_INFRA-2008-1.1.1 Number 226507-NMI3. Additionally, the author would like to thank M.J. Zuber for his helping hand in graphical issues.

References

Bacon, G.E. (1975). *Neutron Diffraction*. Oxford, UK: Clarendon Press.

Cerezo, A. & Davin, L. (2007). Aspects of the observation of clusters in the 3-dimensional atom probe. *Surf Interf Anal* **39**(2–3), 184–188.

Charleux, M., Livet, F., Bley, F., Louchet, F. & Bréchet, Y. (1996). Thermal ageing of an Fe-Cu alloy: Microstructural evolution and precipitation hardening. *Phil Mag A* **73**(4), 883–897.

Dahmen, U., Ferguson, P. & Westmacott, K.H. (1984). Invariant line strain and needle-precipitate growth directions in Fe-Cu. *Acta Metallurg* **32**(5), 803–810.

Deschamps, A., Militzer, M. & Poole, W.J. (2001). Precipitation kinetics and strengthening of a Fe-0.8wt%Cu alloy. *ISIJ Int* **41**(2), 196–205.

Goodman, S.R., Brenner, S.S. & Low, J.R. (1973*a*). An FIM-atom probe study of the precipitation of copper from lron-1.4 at. pct copper. Part I: Field-ion microscopy. *Metallurg Trans* **4**(10), 2363–2369.

Goodman, S.R., Brenner, S.S. & Low, J.R. (1973*b*). An FIM-atom probe study of the precipitation of copper from iron-1.4 at. pct copper. Part II: Atom probe analyses. *Metallurg Trans* **4**(10), 2371–2378.

Haasen, P. (1978). *Physical Metallurgy*, Mordike, J. (translator). Cambridge, UK; New York: Cambridge University Press.

Hellman, O.C., Vandenbroucke, J.A., Rüsing, J., Isheim, D. & Seidman, D.N. (2000). Analysis of three-dimensional atom-probe data by the proximity histogram. *Microsc Microanal* **6**(5), 437–444.

Hornbogen, E. (1962). The role of strain energy during precipitation of copper and gold from alpha iron. *Acta Metallurg* **10**(5), 525–533.

Hornbogen, E. & Glenn, R.C. (1960). A metallographic study of precipitation of copper from alpha iron. *Trans Metallurg Soc AIME* **218**, 1064–1070.

Isheim, D., Gagliano, M.S., Fine, M.E. & Seidman, D.N. (2006). Interfacial segregation at Cu-rich precipitates in a high-strength low-carbon steel studied on a sub-nanometer scale. *Acta Mater* **54**(3), 841–849.

Isheim, D. & Seidman, D.N. (2004). Nanoscale studies of segregation at coherent heterophase interfaces in alpha-Fe based systems. *Surf Interf Anal* **36**(5–6), 569–574.

Kostorz, G. (1979). In treatise on materials science and technology. *Neutron Scattering*, Kostorz, G. (Ed.), vol. 15, pp. 226–228. New York: Academic Press.

Lahiri, S.K., Chandra, D., Schwartz, L.H. & Fine, M.E. (1969). Modulus and Moessbauer studies of precipitation in Fe-1.67 at.% Cu. *Met Soc AIME-Trans* **245**(9), 1865–1868.

Leitner, H., Clemens, H., Akre, J., Danoix, F. & Staron, P. (2007). On the evolution of secondary hardening carbides in a high-speed steel characterised by APFIM and SANS. *Int J Mater Res* **98**(11), 1093–1103.

Leitner, H., Stiller, K., Andren, H.O. & Danoix, F. (2004). Conventional and tomographic atom probe investigations of secondary-hardening carbides. *Surf Interf Anal* **36**(5–6), 540–545.

Liu, J.Z., Van De Walle, A., Ghosh, G. & Asta, M. (2005). Structure, energetics, and mechanical stability of Fe-Cu bcc alloys from first-principles calculations. *Phys Rev B* **72**(14), 1–16.

Maruyama, N., Sugiyama, M., Hara, T. & Tamehiro, H. (1999). Precipitation and phase transformation of copper particles in low alloy ferritic and martensitic steels. *Mater Trans JIM* **40**(4), 268–277.

Mathon, M.H., Barbu, A., Dunstetter, F., Maury, F., Lorenzelli, N. & De Novion, C.H. (1997). Experimental study and modelling of copper precipitation under electron irradiation in dilute FeCu binary alloys. *J Nucl Mater* **245**(2–3), 224–237.

Miller, M.K. (1996). *Atom Probe Field Ion Microscopy*. Oxford, New York: Clarendon Press, Oxford University Press.

Miller, M.K., Pareige, P. & Burke, M.G. (2000). Understanding pressure vessel steels: An atom probe perspective. *Mater Charac* **44**(1–2), 235–254.

Miller, M.K., Wirth, B.D. & Odette, G.R. (2003). Precipitation in neutron-irradiated Fe-Cu and Fe-Cu-Mn model alloys: A comparison of APT and SANS data. *Mater Sci Eng A* **353**(1–2), 133–139.

Morley, A., Sha, G., Hirosawa, S., Cerezo, A. & Smith, G.D.W. (2009). Determining the composition of small features in atom probe: bcc Cu-rich precipitates in an Fe-rich matrix. *Ultramicroscopy* **109**(5), 535–540.

Osamura, K., Okuda, H., Takashima, M., Asano, K. & Furusaka, M. (1993). Small-angle neutron scattering study of phase decomposition in Fe-Cu binary alloy. *Mater Trans JIM* **34**(4), 305–311.

Othen, P.J., Jenkins, M.L., Smith, G.D.W. & Phythian, W.J. (1991). Transmission electron microscope investigations of the structure of copper precipitates in thermally-aged Fe-Cu and Fe-Cu-Ni. *Phil Mag Lett* **64**(6), 383–391.

Pareige, P., Auger, P., Bas, P. & Blavette, D. (1995). Direct observation of copper precipitation in a neutron irradiated FeCu alloy by 3D atomic tomography. *Scripta Metall Mater* **33**(7), 1033–1036.

Pareige, P. & Miller, M.K. (1996). Characterization of neutron-induced copper-enriched clusters in pressure vessel steel weld: An APFIM study. *Appl Surf Sci* **94–95**, 370–377.

Pareige, P.J., Russell, K.F. & Miller, M.K. (1996). APFIM studies of the phase transformations in thermally aged ferritic FeCuNi alloys: Comparison with aging under neutron irradiation. *Appl Surf Sci* **94–95**, 362–369.

Pareige, P., Russell, K.F., Stoller, R.E. & Miller, M.K. (1997*a*). Influence of long-term thermal aging on the microstructural evolution of nuclear reactor pressure vessel materials: An atom probe study. *J Nucl Mater* **250**(2–3), 176–183.

Pareige, P., Stoller, R.E., Russell, K.F. & Miller, M.K. (1997*b*). Atom probe characterization of the microstructure of nuclear pressure vessel surveillance materials after neutron irradiation and after annealing treatments. *J Nucl Mater* **249**(2–3), 165–174.

Prakash Kolli, R. & Seidman, D.N. (2008). The temporal evolution of the decomposition of a concentrated multicomponent Fe-Cu-based steel. *Acta Mater* **56**(9), 2073–2088.

Schober, M., Eidenberger, E., Leitner, H., Staron, P., Reith, D. & Podloucky, R. (2010). A critical consideration of magnetism and composition of (bcc) Cu precipitates in (bcc) Fe. *Appl Phys A* **99**, 697–704.

Smith, C.S. & Palmer, E.W. (1933). Precipitation hardening of copper steels. *Trans AIME* **105**, 133–168.

Vaumousse, D., Cerezo, A. & Warren, P.J. (2003). A procedure for quantification of precipitate microstructures from three-dimensional atom probe data. *Ultramicroscopy* **95**, 215–221.

Worrall, G.M., Buswell, J.T., English, C.A., Hetherington, M.G. & Smith, G.D.W. (1987). A study of the precipitation of copper particles in a ferrite matrix. *J Nucl Mater* **148**(1), 107–114.

Zhang, W. & Ma, E. (2000). Magnetic moment and atomic volume in supersaturated Fe-Cu solid solutions: *Ab initio* calculations compared with experiments. *J Mater Res* **15**(3), 653–658.